# Supplementary Information

## Table of Contents

## 1. Supplementary Table

Table S1. Fitting parameters for the equivalent circuit model for selected AEMFCs at a current density of 0.1 $A \cdot cm^{-2}$.

| **Membrane (Thickness)** | **FAA-3-50 (50 µm)** | **FAA-3-50 (50 µm)** | **QPC-TMA-Ann (50 µm)** |
|---|---|---|---|
| **Ionomer** | **FAA-3** | **QPC-TMA** | **QPC-TMA** |
| **L** | $3.320 \times 10^{-7}$ | $1.670 \times 10^{-7}$ | $3.102 \times 10^{-7}$ |
| **$R_{Ohm}$** | 0.0898 | 0.0809 | 0.0567 |
| **$R_{CT,\ Anode}$** | 0.1083 | 0.0332 | 0.0409 |
| **$CPE_{anode}$-T, P** | 0.1695, 0.5437 | 0.1016, 0.6726 | 0.0604, 0.7074 |
| **$R_{CT,\ Cathode}$** | 0.4066 | 0.3568 | 0.3433 |
| **$CPE_{Cathode}$-T, P** | 0.0733, 0.9432 | 0.0536, 0.9583 | 0.0556, 0.9609 |

**Table S2. Summary of AEMWE performance at 1.9 V reported in literature.**

| Reference | Year | Anode catalyst | Membrane | Cathode catalyst | Cell temperature [°C] | Performance [mA $cm^{-2}$] |
|---|---|---|---|---|---|---|
| 50 | 2011 | $Cu_{0.7}Co_{2.3}O_4$ | mm-qPVBz/$Cl^-$ | Pt black | 25 | 120 |
| 51 | 2012 | $IrO_2$ | A201 | Ni-Mo | 50 | 555 |
| 52 | 2013 | Graphene | Selemion AMV | Graphene | 80 | 150 |
| 53 | 2014 | Ni/$CeO_2$-$La_2O_3$/C | A-201 | $CuCoO_3$ | 50 | 470 |
| 1 | 2015 | Ni/$CeO_2$-$La_2O_3$/C | PSF Quaternary ammonium | $CuCoO_3$ | 70 | 120 |
| 54 | 2017 | $IrO_2$ | A-201 | 46.5 wt.% Pt/C | 50 | 360 |
| 26 | 2018 | g-CN-CNF | FAA-3-50 | 40 wt.% Pt/C | 60 | 726 |
| 27 | 2019 | $IrO_2$ | FAA-3-50 | 40 wt.% Pt/C | 70 | 1500 |
| 55 | 2019 | $IrO_2$ | LSCPi | Pt/C | 50 | 450 |
| 56 | 2020 | Ir | Aemion | 60 wt.% Pt/C | 50 | 1800 |
| 57 | 2020 | $IrO_2$ | HTMA | 50 wt.% PtRu/C | 85 | 1900 |
| **This work** | **2020** | **$IrO_2$** | **QPC-TMA** | **40 wt.% Pt/C** | **70** | **3495** |

## 2. Supplementary Discussion

### 2.1 Polymer synthesis and rheological property

The synthesized monomers and polymers are characterized by $^{1}$H-NMR and $^{13}$C-NMR spectroscopy. The proton peak at 3.31 ppm originating from $CH_2Br$ disappears completely from the $^{1}$H-NMR spectrum of PC-br. Then, the new proton peaks, which should signify the introduction of ion conducting groups, appear at 3.19 and 3.50 ppm on the $^{1}$H-NMR spectroscopy of QPC-TMA (**Figure S2**).

**9-(6-Bromohexyl)-9H-carbazole (BHC)**

The chemical structure of BHC was confirmed by $^{1}$H NMR. $^{1}$H NMR (500 MHz, $CDCl_3$-$d_1$) d (ppm): 8.02 ($H_1$), 7.38 ($H_2$), 7.31 ($H_3$), 7.15 ($H_4$), 4.21 ($H_5$), 3.26 ($H_6$), 1.80 ($H_7$), 1.71 ($H_8$), 1.38 ($H_9$), and 1.30 ($H_{10}$). $^{13}$C NMR (75 MHz, $CDCl_3$-$d_1$) d (ppm): 140.45, 125.67, 122.90, 120.44, 118.85, 108.67, 42.89, 33.82, 32.63, and 26.52.

**Poly(carbazole)-based polymer (poly(9-(6-bromohexyl)-9H-carbazole-*co*-1,1,1-trifluoroisopropane) (Pc-br)**

The chemical structure of PC-br was confirmed using $^{1}$H NMR. $^{1}$H NMR (500 MHz, DMF-$d_7$) d (ppm): 8.31 (Ha), 7.45 (Hb), 7.22 (Hc), 4.23 (Hd), 3.29 ($H_i$), 2.05 ($H_j$), 1.76–1.53 ($H_e$, $H_h$), and 1.38–1.20 ($H_f$, $H_g$). $^{13}$C NMR (75 MHz, DMF-$d_7$) d (ppm): 162.21, 140.10, 133.33, 129.95, 122.62, 109.32, 54.28, 54.15, 42.96, 32.89, 29.05, 27.91, 26.28, and 24.96.

**Quaternised poly(carbazole)-based polymer (poly(9-(6-(trimethylammonium bromide)hexyl)-9H-carbazole-co-1,1,1-trifluoroisopropane) (QPC-TMA)**

The chemical structure of QPC-TMA was confirmed by $^{1}$H NMR. $^{1}$H NMR (500 MHz, DMF-$d_7$) d (ppm): 8.67 ($H_{a'}$), 7.92 ($H_{b'}$), 7.52 ($H_{c'}$), 4.67 ($H_{d'}$), 3.66 ($H_{i'}$), 3.34 ($H_k$), 2.19 ($H_{j'}$), 1.90-1.72 ($H_{e'}$, $H_{h'}$), 1.53–1.34 ($H_{f'}$, $H_{g'}$). $^{13}$C NMR (75 MHz, DMF-$d_7$) d (ppm): 162.21, 140.09, 133.27, 129.95, 128.34, 122.53, 65.84, 54.25, 54.12, 52.45, 28.88, 26.32, 26.02, 24.92, and 22.58.

## 2.2. Detail description about the EIS spectra of AEMFC

To quantitatively explain the EIS spectra, the EIS data were fitted based on the equivalent circuit shown in Figure R8. A good agreement between experimental results (points) and fitted data (solid lines) shows the validity of the model. One thing to mention here is that the EIS fitting was only conducted for the EIS spectra measured at kinetic region (0.1 A $cm^{-2}$), where the effect of mass transport can be ignored. This is because, at anode of AEMFC, hydrogen oxidation reaction requires a considerable overpotential and mass transport problems occur, such as water flooding and limited hydrogen diffusion by adsorbed ionomer. Therefore, it is difficult to separate the EIS curve of the two electrodes under the operating condition where the effects of mass transport cannot be ignored.

At kinetic region, both MEAs showed two distinct capacitive loops at high (with time constant of ~ 1 kHz) and inter-mediate frequencies (with time constant of ~ 10 Hz) associated with hydrogen oxidation and oxygen reduction, respectively. This result matches well with the previous work reported by Reshetenko et al.[1] The total charge transport resistance of the QPC-TMA-based MEA (~ 0.384 Ω $cm^2$) were 25.5 % lower than those of the FAA-3-based MEA (~ 0.515 Ω $cm^2$). Especially, despite the use of FAA-3 membranes instead of QPC-TMA membrane, MEA using the QPC-TMA electrodes exhibits same charge transport resistance (~ 0.390 Ω $cm^2$) (Figure S5). According to the fitted result, when using the QPC-TMA ionomer instead of the FAA-3 ionomer, the charge transport resistances at both electrodes decreases. In particular, the decrease in charge transport resistance of the anode is more compared to that of the cathode. This is because QPC-TMA inhibits ionomer adsorption that occurs primarily at the anode. In addition, as shown in the Figure R9, the peak frequency of the capacitive loop of the QPC-TMA cathode is higher than that of the FAA-3 cathode, which is another reason for the higher activity of the QPC-TMA electrode.

In addition to improved kinetic of QPC-TMA electrode (Figure S8), the superior properties of QPC-TMA ionomer are beneficial to mass transport in the electrode. In the case of FAA-3-based MEA (Figure S9), a low frequency arc (with a time constant of ~ 1 Hz) appears at the current density of 0.8 A $cm^{-2}$, which indicates that mass transport affects the electrode reaction. It is notable that the FAA-3-based MEA shows noticeably the low-frequency arc, whereas the QPC-TMA-ionomer based MEAs do not show such arc despite the membrane used. This is because the QPC-TMA ionomer has higher ionic conductivity and prevent the ionomer adsorption on platinum, thereby facilitating mass transport to the electrode surface. As the operating current increases (1.2 A $cm^{-2}$ at 0.6V), the FAA-3-based MEA showed the considerably large low frequency arc. On the other hand, the QPC-TMA-based MEA

exhibited the much smaller low frequency arc compared to that of the FAA-3-based one despite the 2-fold higher operating current (2.5 A $cm^{-2}$) at 0.6 V thanks to the excellent properties of the QPC-TMA ionomer.

## 2.3. Effect of QPC-TMA ionomer in AEMWE

AEMWEs prepared with different QPC-TMA ionomer contents were evaluated to determine the optimized ionomer content in the catalyst layer. **Figure S10a** presents the polarization curves of the AEMWEs with different contents of 5, 10, 15, 20, 25, and 30 wt.% in the anode. The cell performance increased as the content of the QPC-TMA ionomer increased from 5 to 10 wt.%. When the ionomer content was higher than 10 wt.%, the increased ionomer content reduced the cell performance. This phenomenon is attributed to the effect of the charge-transfer resistance, rather than the effect of ohmic resistance, as shown in the EIS curves conducted at 1.9 V (**Figure S10b**). For the polymer-electrolyte membrane fuel cells (PEMFCs), a higher ionomer content in the catalyst layer reduces the ohmic resistance.[2, 3] It can be expected that different ionomer contents influenced the ohmic resistance of AEMWE to a different extent. Contrary to this expectation, the ohmic resistance of AEMWEs prepared with the different ionomer contents was constant. This is because excess reactant was supplied to anode, leading to efficient ion transfer. On the other hand, different ionomer contents impacted the charge-transfer resistance. Low ionomer contents led to a dense catalyst layer with smaller secondary pores.[4] Excessive contents increased the charge-transfer resistance by covering the active site of the electrochemical catalyst. As illustrated in **Figure S10b**, the ionomer content of 10 wt. % was sufficient to minimize the charge-transfer resistance. As a result, the optimal content required to attain high AEMWE performance in the anode was determined to be 10 wt.%.

**Figure S10** shows the performance of the AEMWE applied with different ionomers (QPC-TMA and FAA-3 ionomers) in the anode. As shown in **Figure S10c**, the AEMWE using the QPC-TMA ionomer showed better performance than that using the FAA-3 ionomer, which is due to its low ohmic resistance **(Figure S10d)**. This is because the QPC-TMA ionomer has a high ionic conductivity compared with the FAA-3 ionomer, as illustrated in Table S1. In addition, the Nyquist plot reveals that the charge-transfer resistance of AEMWE with the QPC-TMA ionomer was smaller than that with the FAA-3 ionomer, which is due to the larger secondary pore in the catalyst layer. Figure S10e presents the size distribution of catalyst agglomerates in the two types of slurry prepared with the QPC-TMA and FAA-3 ionomers. The average sizes of the agglomerates in the slurry with the FAA-3 and QPC-TMA ionomers were 325.3 and 202.7 nm, respectively. When prepared with the QPC-TMA ionomer, the catalyst layer was composed of agglomerates of smaller sizes, leading to more porous electrodes, as shown in **Figure S10f-g**.[5-7] In other words, the larger secondary pores in the catalyst layer reduced the charge-transfer resistance.[8,9] Therefore, the

use of the QPC-TMA ionomer resulted in an enhanced cell performance due to its reduced ohmic and charge-transfer resistance.

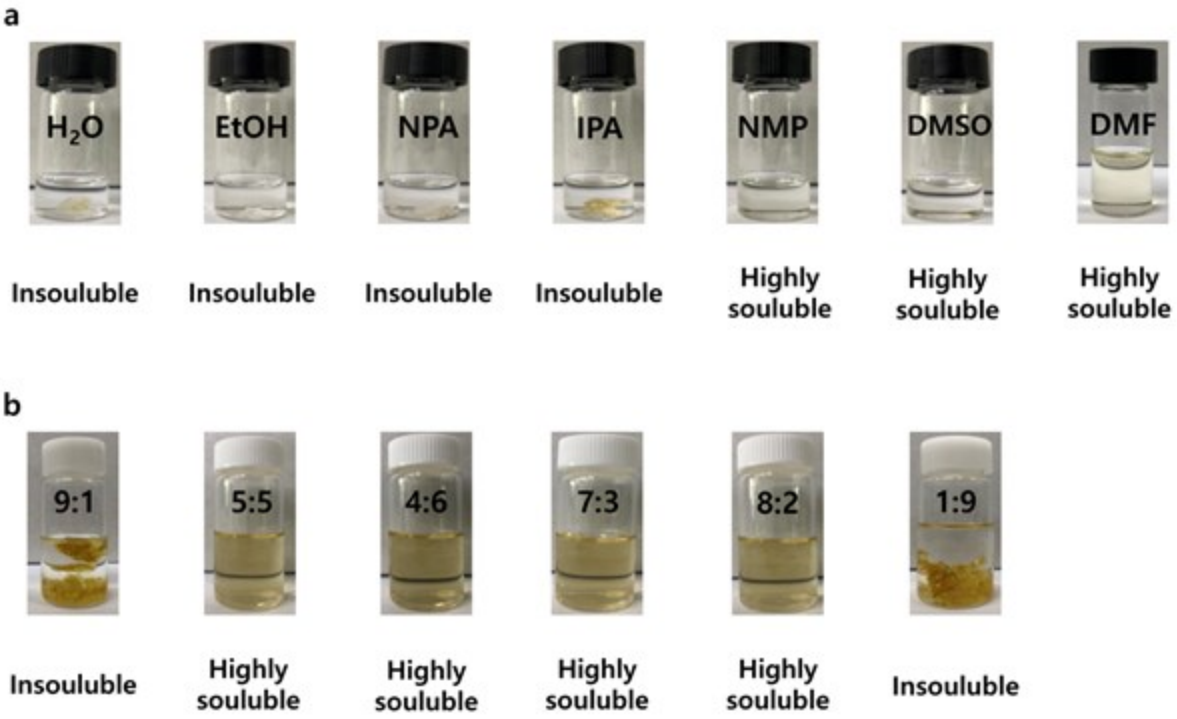


**Figure S1.** Solubility test of QPC-TMA ionomer at (a) typical protic or aprotic polar solvents and (b) mixed solvent ($H_2O$:NPA). the QPC-TMA is dissolved in polar aprotic solvents such as DMF, NMP, DMSO, and NPA/$H_2O$ mixed solvent; it is proposed that the synthesized polymer could function as an electrode binder

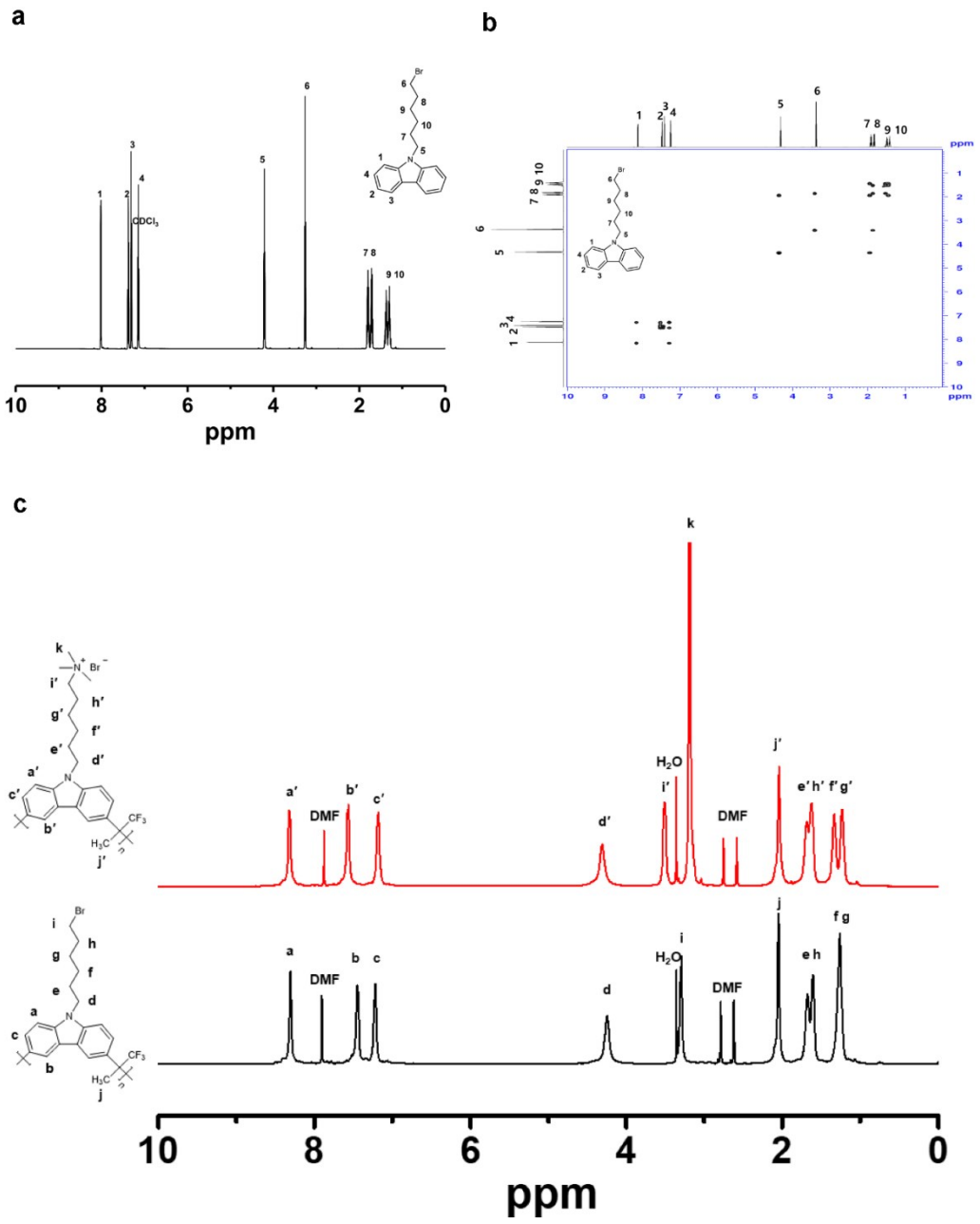


**Figure S2. $^1$H NMR spectrum of the monomer and the polymer using $CDCl_3$-$d_1$ and DMF-$d_7$ as the NMR solvent.** (a) $^1$H NMR, (b) COZY spectrum of BHC, and **c**, the comparison of characteristic peaks in $^1$H NMR spectra between PC-Br (black line) and QPC-TMA (red line).

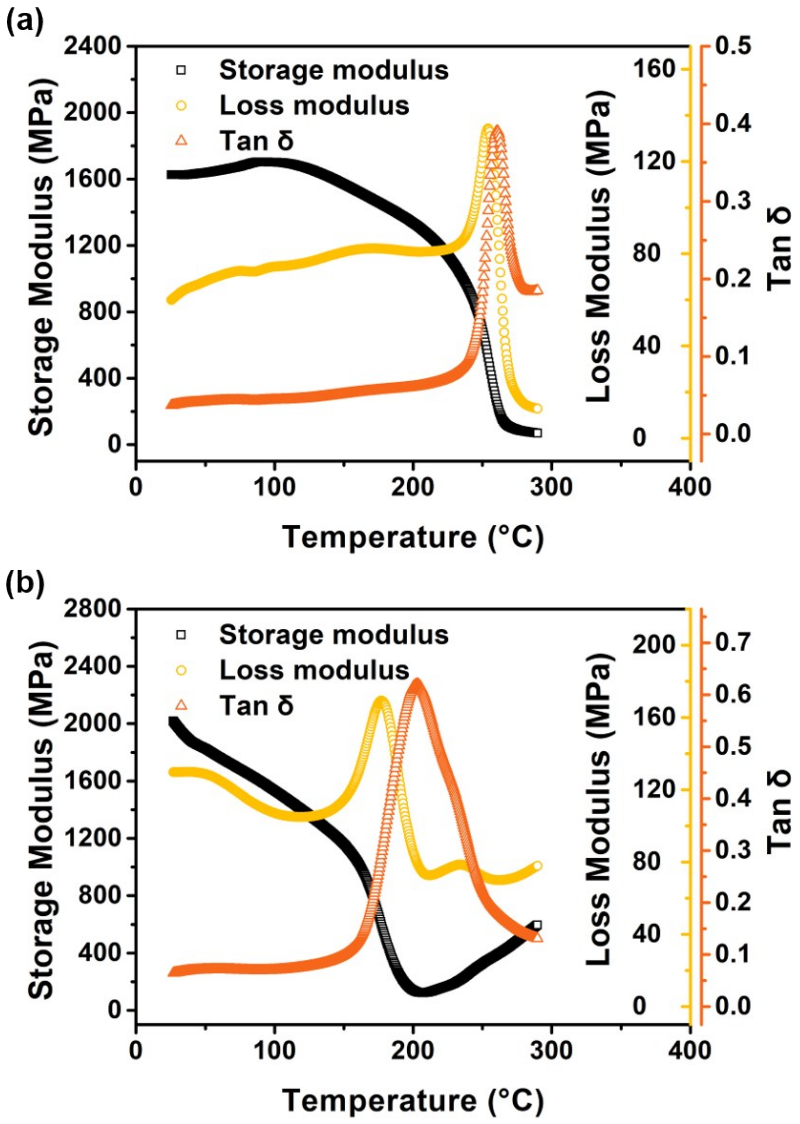


**Figure S3.** Dynamic mechanical analysis (DMA) profiles for (a) QPC-TMA and (b) FAA-3 under 20% RH conditions.

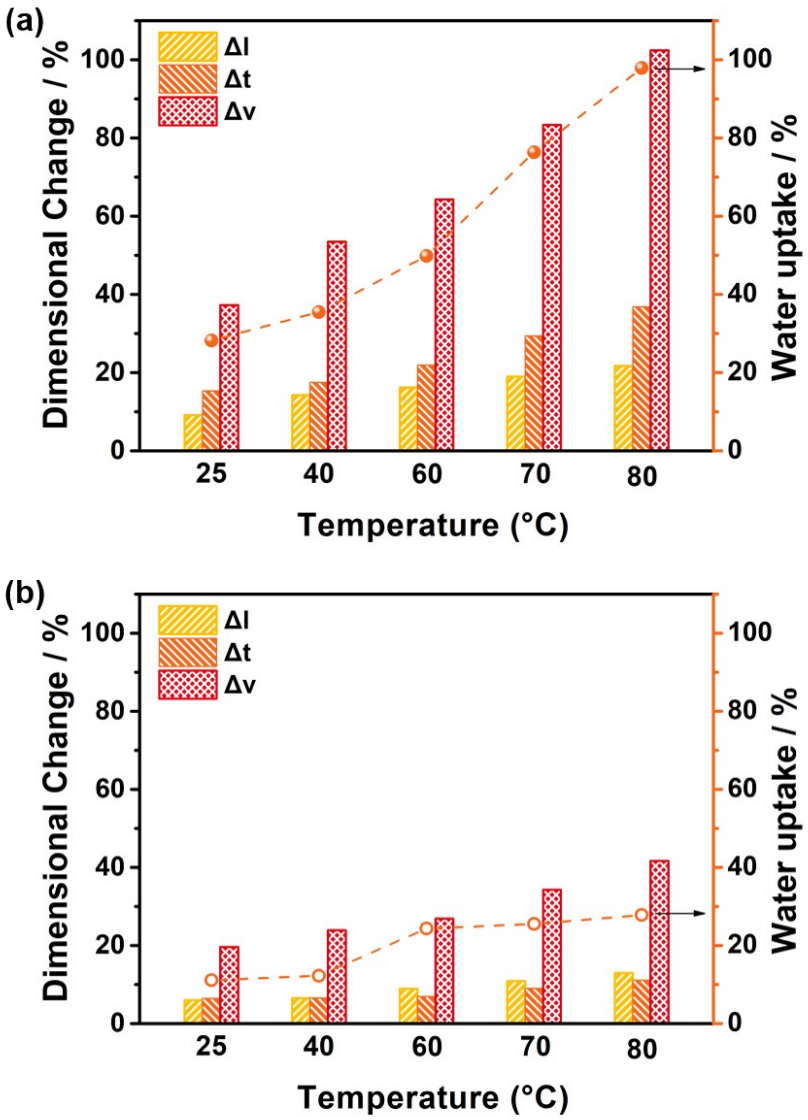


**Figure S4.** Water absorption behaviour of (a) QPC-TMA membrane and (b) FAA-3. The circle symbol depicts the water uptake of AEMs. The dimensional variations of both AEMs increase gradually with an increase in temperature.

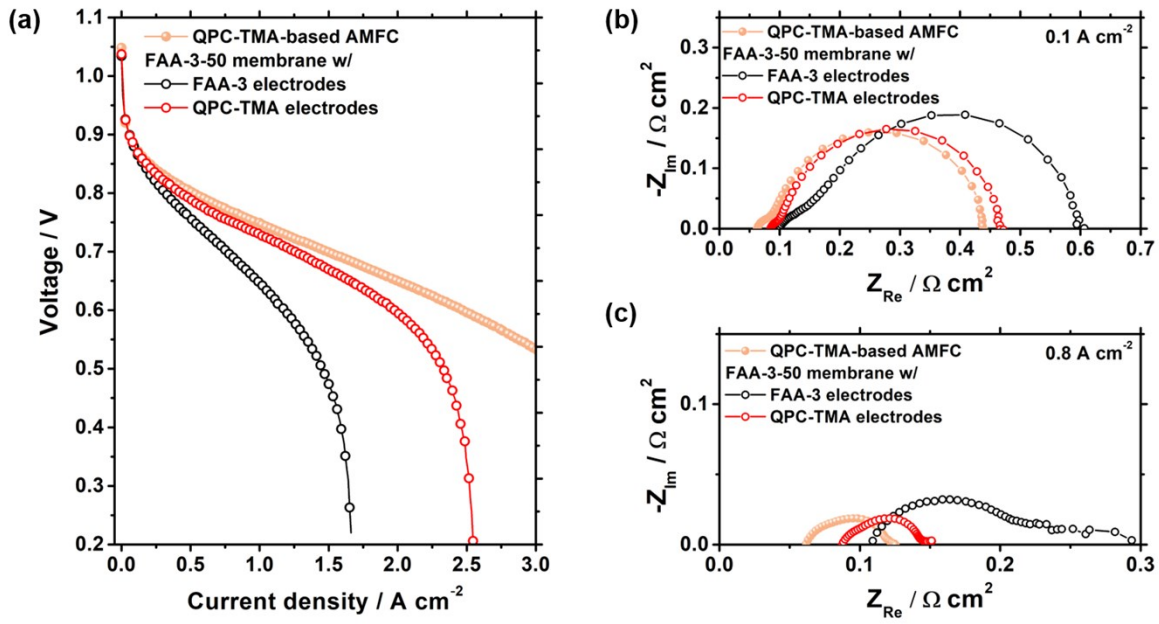


**Figure S5.** (a) Single cell performance of four FAA-3-50 membrane-based MEAs with FAA-3 and QPC-TMA electrodes at 60 °C. All MEA components were the same except for the ionomer in electrodes. PtRu/C and Pt/C were used as the anode and cathode catalysts, respectively, and the precious metal loadings for both electrodes were fixed at 0.4 mg·cm$^{-2}$. (b-c) EIS spectra of four AEMFCs at different single-cell operating currents.

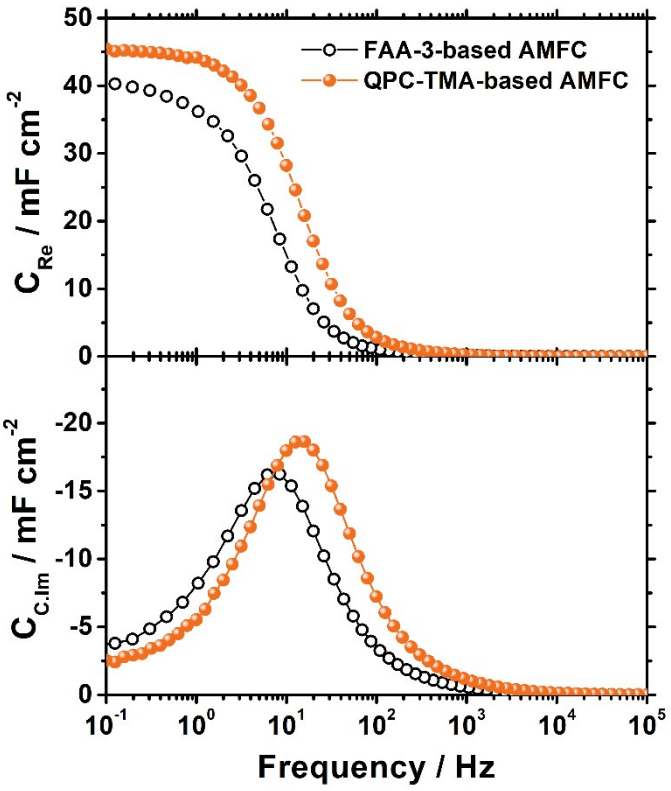


**Figure S6. Complex capacitance analysis for the QPC-TMA and the FAA-3 electrodes.** real part and imaginary part of complex capacitances as a function of the log scale frequency of the cathodes of the two MEAs at non-faradaic conditions.

Test condition: Fully humidified hydrogen and nitrogen were fed into the anode and cathode, respectively, and the single cell temperature was maintained at 30 °C. At this non-faradaic condition, EIS was measured at 0.45 V with an amplitude of 5 mV using the Pt/C cathode as the working electrode and PtRu/C anode as the counter electrode. The measurement was conducted in the frequency range of 100 mHz–100 kHz.

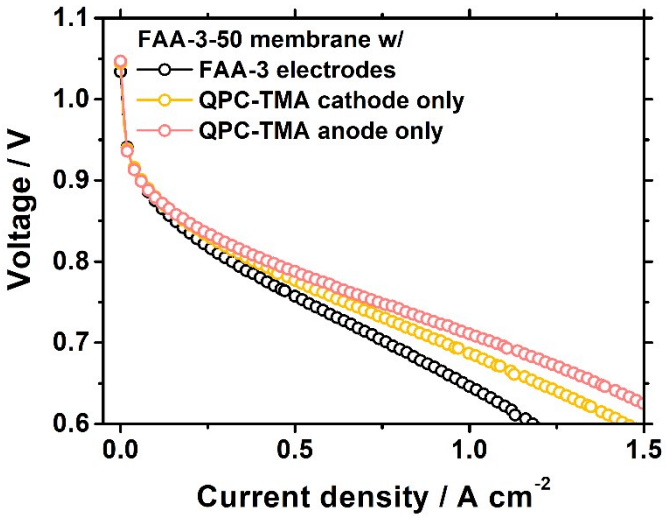


**Figure S7.** Single cell performance of three FAA-3-50 membrane-based MEAs with different ionomer combinations (FAA-3 and QPC-TMA) at 60 °C. All MEA components were the same except for the ionomer in electrodes. PtRu/C and Pt/C were used as the anode and cathode catalysts, respectively, and the precious metal loadings for both electrodes were fixed at 0.4 mg·cm$^{-2}$.

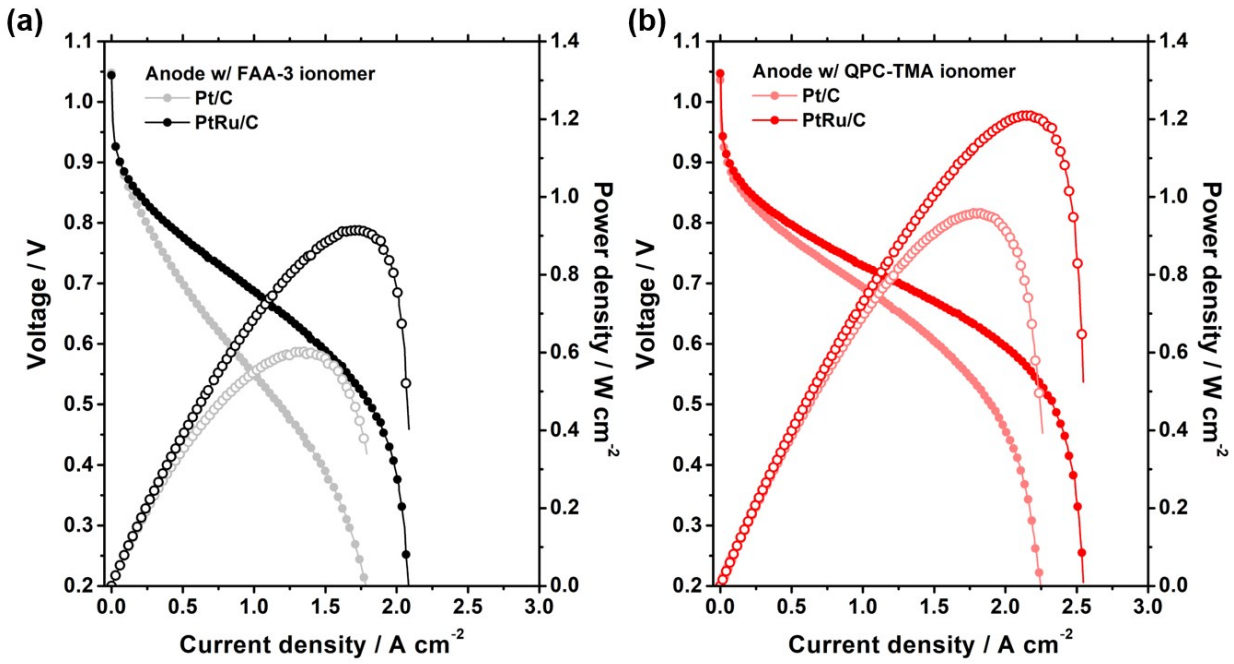


**Figure S8.** Single cell performance of four FAA-3-50 membrane-based MEAs with anode ionomer (FAA-3 and QPC-TMA) and catalyst (Pt/C and PtRu/C) combinations at 60 °C. All MEA components were the same except for the anode. PtRu/C and Pt/C were used as the anode and cathode catalysts, respectively, and the precious metal loadings for both electrodes and ionomer to carbon weight ratio were fixed at 0.4 mg·cm$^{-2}$ and 0.5, respectively. The QPC-TMA ionomer used for cathode ionomer.

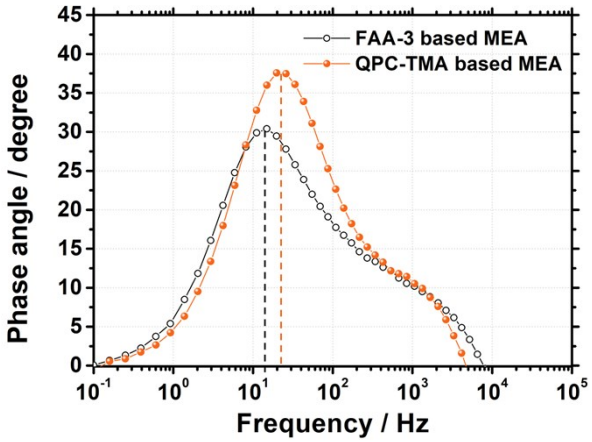


**Figure S9.** Bode-phase angle plot for the measured EIS spectra of the QPC-TMA-based and (b) FAA-3-based AEMFCs at 0.1 A·cm$^{-2}$

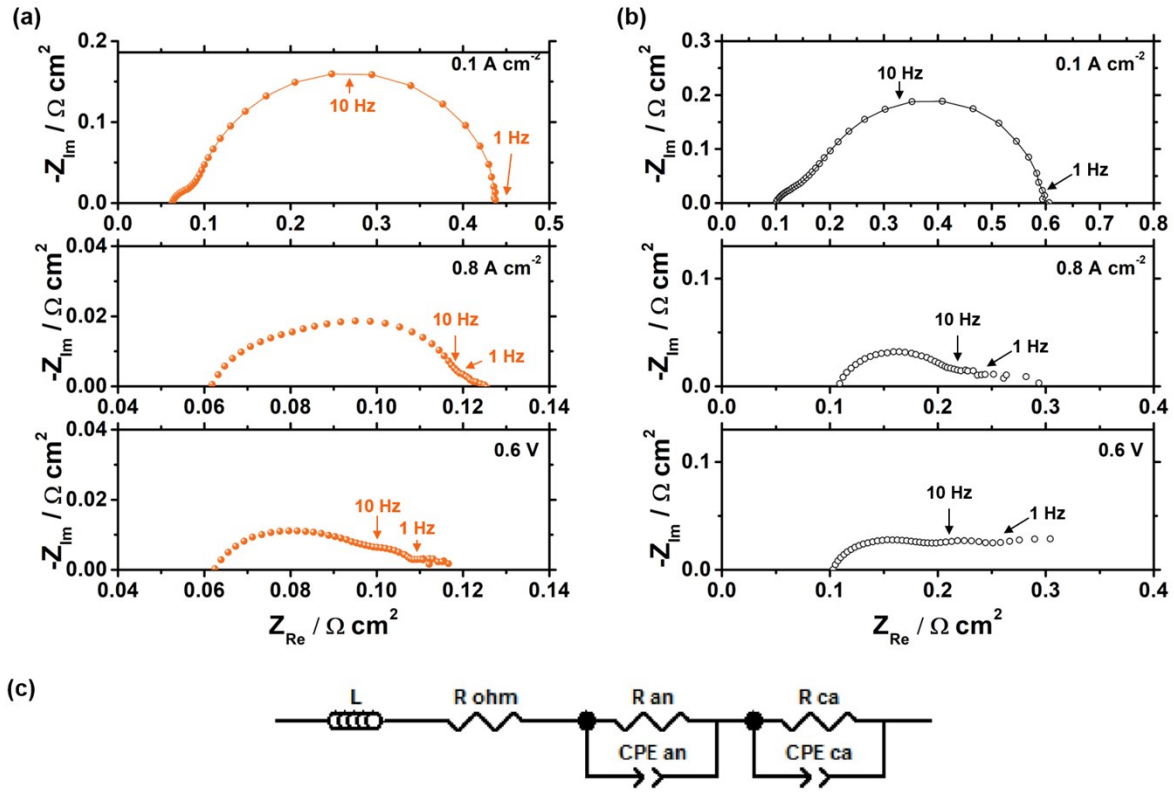


**Figure S10.** Detailed EIS spectra of the (a) QPC-TMA-based and (b) FAA-3-based AEMFCs at different single-cell operating currents and voltage. (c) Equivalent circuit model used for EIS fitting for Table S1.

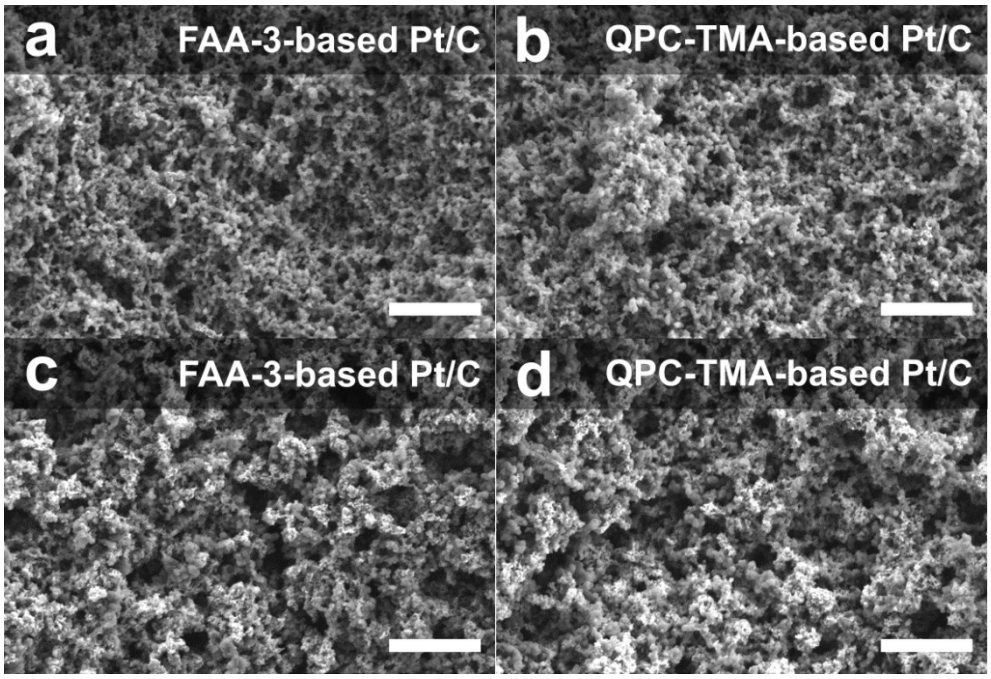


**Figure S11.** FE-SEM images of the electrodes of (a) FAA-3 ionomer-based Pt/C, (b) QPC-TMA ionomer-based Pt/C, (c) FAA-3 ionomer-based PtRu/C, and (d) QPC-TMA ionomer-based PtRu/C. The scale bar is 1 μm.

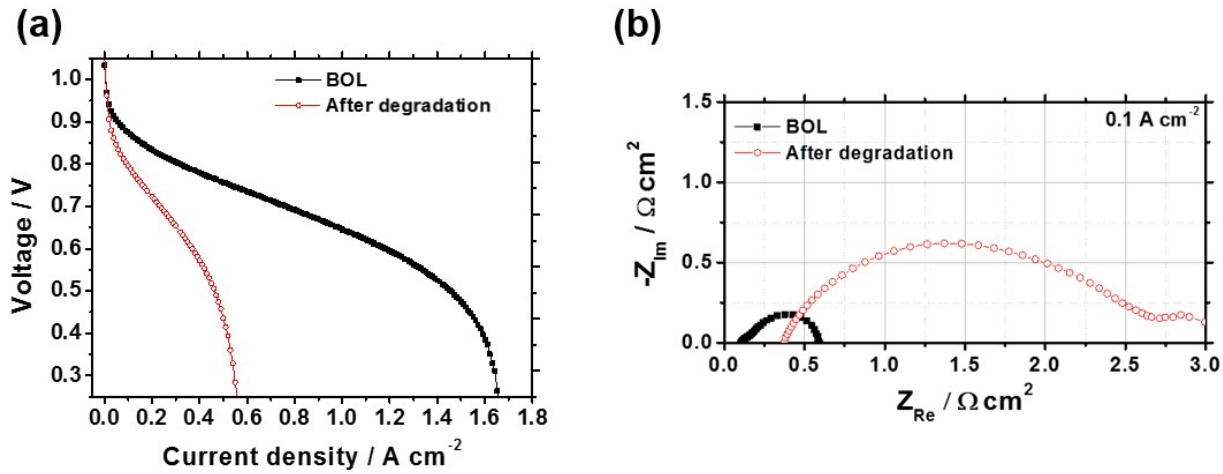


**Figure S12.** (a) Single cell performance and (b) EIS spectra at 0.1 A $cm^{-2}$ of the FAA-3-based MEA before and after cell degradation

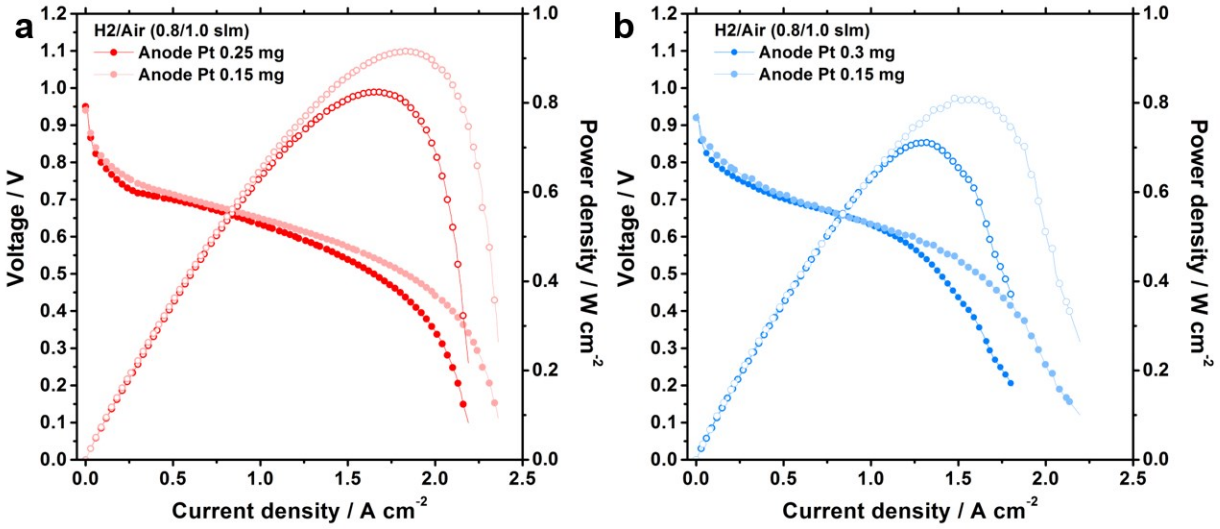


**Figure S13.** Single cell performance of two QPC-TMA-based AEMFCs using **(a)** silver-based cathode and **(b)** Fe,Cu-N co-doped carbon-based cathode tested with $H_2$/Air at 80 °C. Test conditions: non-precious metal-based cathode (2 mg·cm$^{-2}$) and a low-Pt anode using 30 wt.% PtRu/C (Johnson Matthey Co., USA) (~ 150 μg·cm$^{-2}$). Humidified hydrogen (0.8 L·min-1, relative humidity of ~ 90%) and oxygen (1.0 L·min-1, relative humidity of ~90%) were fed into the anode and cathode respectively, with 1.5 bar back pressure. Single cell temperature was maintained at 80 °C.

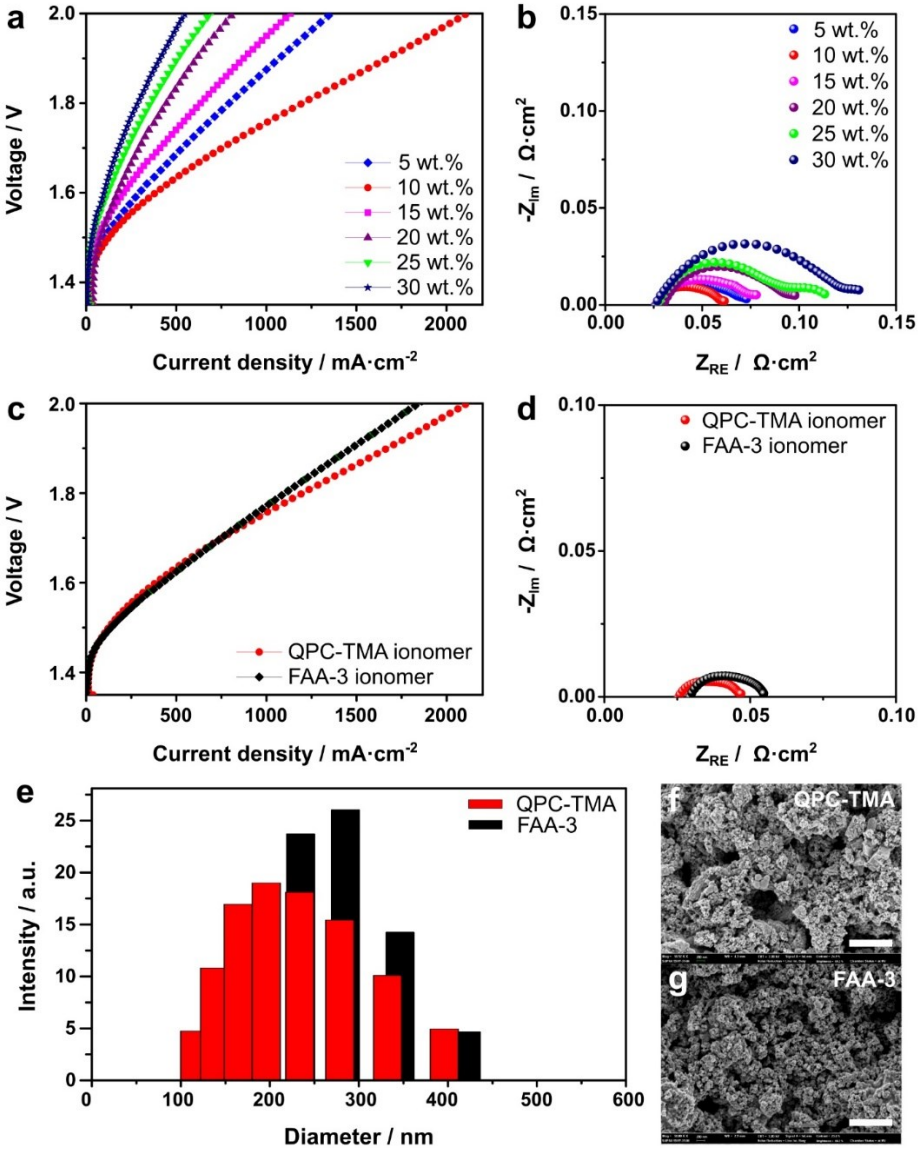


**Figure S14. Effect of QPC-TMA ionomer on AEMWE performance. a**, Polarization curves and **b**, Nyquist plots (1.9 V) of the AEMWEs prepared with varying QPC-TMA ionomer contents of 5, 10, 15, 20, 25, and 30 wt.% in the anode. FAA-3-50-Br ionomer with a content of 30 wt.% was used in the cathode. **c**, Polarization curves and **d**, Nyquist plots (1.9 V) of AEMWEs prepared with QPC-TMA ionomer (10 wt.%) and FAA-3-50-Br ionomer (20 wt.%). FAA-3-50-Br ionomer with a content of 30 wt.% was used in the cathode. **e**, Size distribution of catalyst agglomerates in slurries with QPC-TMA and FAA-3-50-Br ionomer. **f–g**, FE-SEM images of the anode catalyst layer ($IrO_2$) with **f**, QPC-TMA and **g**, FAA-3-50-Br ionomer. The scale bar is 1 μm.

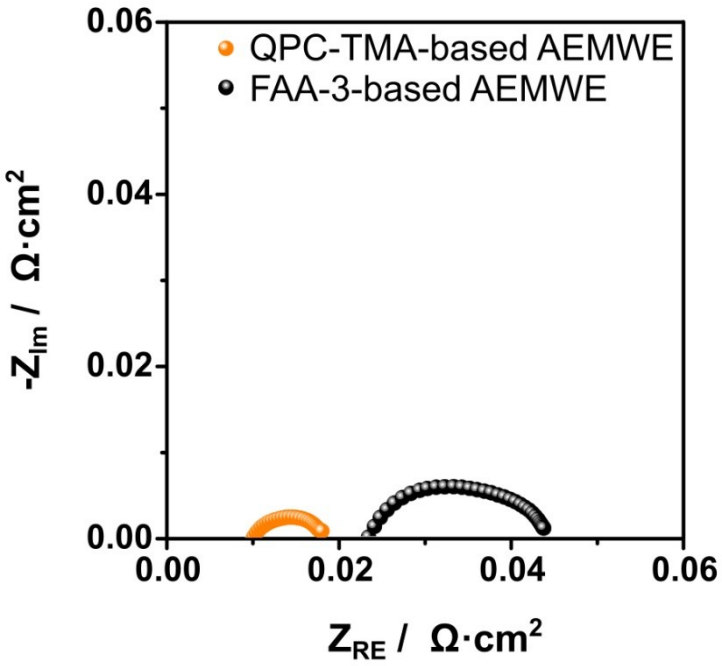


**Figure S15**. **EIS analysis of QPC-TMA-and FAA-3-based AEMWE.** Nyquist plots of QPC-TMA- and FAA-3-based AEMWE obtained at a constant voltage of 1.9 V.

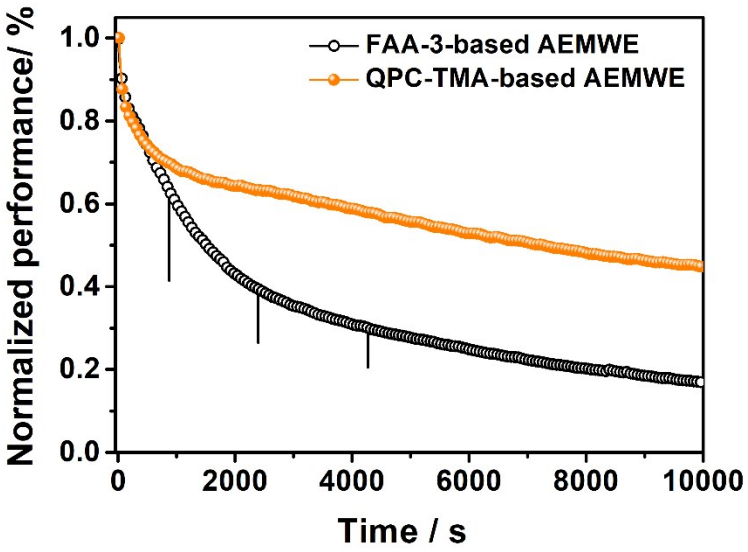


**Figure S16. Comparison of the durability of QPC-TMA-based and FAA-3-based AEMWE.** Single cell durability test of QPC-TMA- and FAA-3-based AEMWE at constant voltage of 1.6 V at 70 °C. The data were normalized based on the initial current (initial) of each AEMWE.

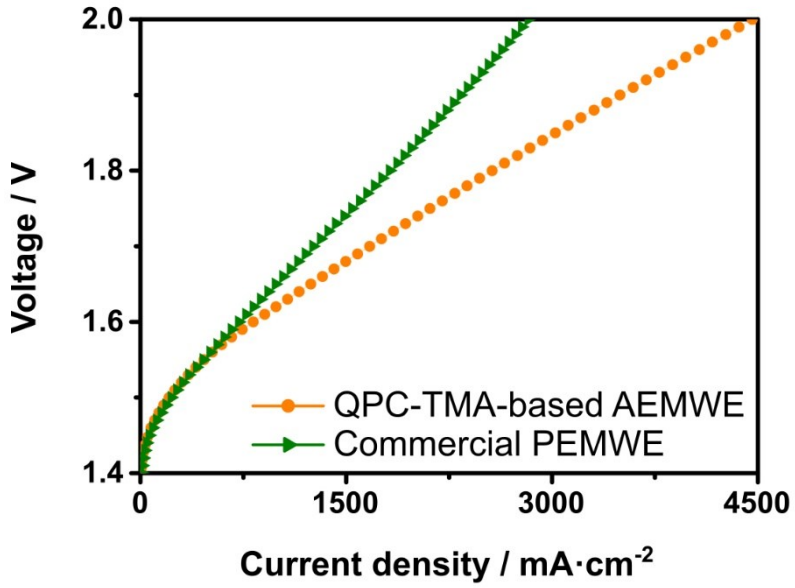


**Figure S17. Comparison of the performance of QPC-TMA-based AEMWE and commercial PEMWE.** Polarization curves of QPC-TMA-based AEMWE and commercial PEMWE. $IrO_2$ with loading of 2.0 mg·cm$^{-2}$ and 40 wt.% Pt/C with loading of 0.4 mg·cm$^{-2}$ were used as the anode and cathode catalyst, respectively. The cell temperature was 70 °C. The feed rate of reactant was 1 mL·min$^{-1}$. The commercial PEMWE is the PEMWE using Nafion membrane and Nafion ionomer. The durability test was conducted at constant voltage of 1.6 V.

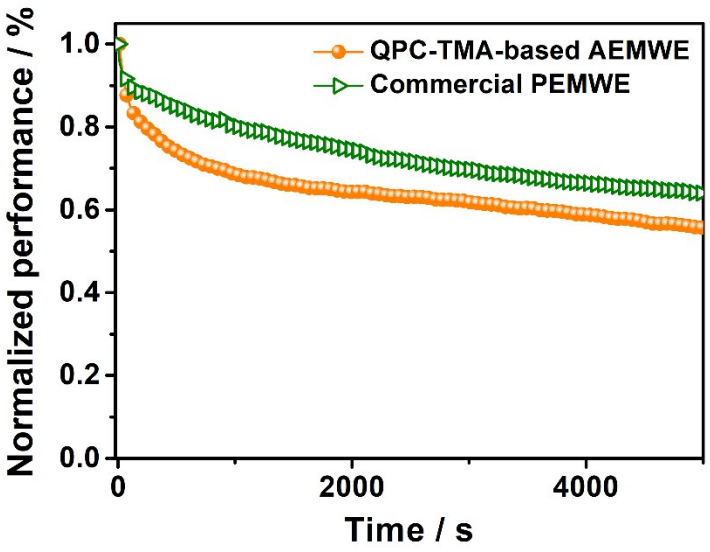


**Figure S18. Comparison of the durability of QPC-TMA-based AEMWE and commercial PEMWE.** Durability of QPC-TMA-based AEMWE and commercial PEMWE conducted at constant voltage of 1.6 V. $IrO_2$ with loading of 2.0 mg·cm$^{-2}$ and 40 wt.% Pt/C with loading of 0.4 mg·cm$^{-2}$ were used as the anode and cathode catalyst, respectively. The feed rate of reactant was 1 mL·min$^{-1}$. The commercial PEMWE is the PEMWE using Nafion membrane and Nafion ionomer. The data were normalized based on the initial current (initial) of each AEMWE.

## ■ REFERENCES


1. T. Reshetenko, M. Odgaard, D. Schlueter, and A. Serov, Journal of Power Sources, 2018, 185-190
2. R. Makharia, M. F. Mathias and D. R. Baker, *Journal of The Electrochemical Society*, 2005, **152**.
3. S. J. Seo, J. J. Woo, S. H. Yun, H. J. Lee, J. S. Park, T. Xu, T. H. Yang, J. Lee and S. H. Moon, *Phys Chem Chem Phys*, 2010, **12**, 15291-15300.
4. J. E. Park, S. Y. Kang, S.-H. Oh, J. K. Kim, M. S. Lim, C.-Y. Ahn, Y.-H. Cho and Y.-E. Sung, *Electrochimica Acta*, 2019, **295**, 99-106.
5. A. Orfanidi, P. J. Rheinländer, N. Schulte and H. A. Gasteiger, *Journal of The Electrochemical Society*, 2018, **165**, F1254-F1263.
6. O. H. Kim, S. H. Oh, C. Y. Ahn, S. Kim, J. K. Kim, J. Kim, S. Yang, M. Choi, Y. H. Cho and Y. E. Sung, *Fuel Cells*, 2018, **18**, 711-722.
7. C.-H. Song and J.-S. Park, *Energies*, 2019, **12**.
8. J. E. Park, S. Kim, O.-H. Kim, C.-Y. Ahn, M.-J. Kim, S. Y. Kang, T. I. Jeon, J.-G. Shim, D. W. Lee, J. H. Lee, Y.-H. Cho and Y.-E. Sung, *Nano Energy*, 2019, **58**, 158-166.
9. S. Shiva Kumar and V. Himabindu, *Materials Science for Energy Technologies*, 2019, **2**, 442-454.